

Learning Dynamic Correlations in Spatiotemporal Graphs for Motion Prediction

Jiajun Fu
Jaakk0F@foxmail.com
School of Artificial Intelligence,
Beijing University of Posts and
Telecommunications
Beijing, China

Fuxing Yang
yangfx@bupt.edu.cn
School of Artificial Intelligence,
Beijing University of Posts and
Telecommunications
Beijing, China

Jianqin Yin*
jqyin@bupt.edu.cn
School of Artificial Intelligence,
Beijing University of Posts and
Telecommunications
Beijing, China

ABSTRACT

Human motion prediction is a challenge task due to the dynamic spatiotemporal graph correlations in different motion sequences. How to efficiently represent spatiotemporal graph correlations and model dynamic correlation variances between different motion sequences is a challenge for spatiotemporal graph representation in motion prediction. In this work, we present Dynamic SpatioTemporal Graph Convolution (DSTD-GC). The proposed DSTD-GC decomposes dynamic spatiotemporal graph modeling into a combination of Dynamic Spatial Graph Convolution (DS-GC) and Dynamic Temporal Graph Convolution (DT-GC). As human motions are subject to common constraints like body connections and present dynamic motion patterns from different samples, we present Constrained Dynamic Correlation Modeling strategy to represent the spatial/temporal graph as a shared spatial/temporal correlation and a function to extract temporal-specific /spatial-specific adjustments for each sample. The modeling strategy represents the spatiotemporal graph with 28.6% parameters of the state-of-the-art static decomposition representation while also explicitly models sample-specific spatiotemporal correlation variances. Moreover, we also mathematically reformulating spatiotemporal graph convolutions and their decomposed variants into a unified form and find that DSTD-GC relaxes strict constraints of other graph convolutions, leading to a stronger representation capability. Combining DSTD-GC with prior knowledge, we propose a powerful spatiotemporal graph convolution network called DSTD-GCN which outperforms state-of-the-art methods on the Human3.6M and CMU Mocap datasets in prediction accuracy with fewest parameters.

KEYWORDS

human motion prediction, spatiotemporal graph convolution, spatiotemporal decomposition, dynamic correlation modeling

1 INTRODUCTION

Human motion prediction is a task of modeling dynamic spatiotemporal correlations between body joints, which plays an increasingly important role in autonomous driving [31], human-machine interaction [17, 41] and healthcare [40].

Traditional methods can handle simple and periodic scenarios with classical time series processing approaches [19, 39], but make unrealistic predictions when human motions become more complex and erratic. Recently, researchers have adopted different deep

learning techniques to human motion prediction, such as Convolution Neural Network (CNN) [20, 23], Recurrent Neural Network (RNN) [2, 8, 10, 20, 26, 30, 30, 33, 35, 38, 42], Generative Adversarial Network (GAN) [4, 9, 12, 14, 18] and Transformer [1, 3]. Although made remarkable improvement when compared with traditional approaches, these methods can't not explicitly model body connections and rely on manual design of filter size for spatial modeling.

Recent studies showed that Graph Convolution Network (GCN) works well on non-grid skeleton data [43] and have been introduced to motion prediction [5, 6, 21, 25, 28, 29, 36]. Mao *et al.* [29] adopt fully-connected GCNs with trainable connectivity. Li *et al.* [21] and Dang *et al.* [6] introduced multi-scale graph connectivity modeling to capture multi-level motions.

Despite the promising results of GCN-based models, there are two challenges for realizing high predictability of human motions: (1) *Lightweight spatiotemporal graph representation*: a human motion sequence is naturally represented as a spatiotemporal graph (see Figure 1 (a)), where spatiotemporal information is precisely stored in the spatiotemporal correlation matrix of quartet space complexity. Although Sofianos *et al.* [36] decompose the spatiotemporal correlation matrix into a combination of temporal-wise spatial correlation matrices and spatial-wise temporal correlation matrices, the space complexity is still nearly cubic. There is still room to explore more parameter-saving decomposition representations of spatiotemporal graph. (2) *Dynamic spatiotemporal correlations*: as illustrated in Figure 1 (b), spatiotemporal correlations are dynamic and vary between input samples. Graph correlations in all previous works [5, 6, 21, 25, 28, 29, 36] adopt static graph correlations as the correlations keep unchanged for all input samples. Although the static correlations are learned through back-propagation and are optimal for all data, they may disturb individual prediction by mistakenly enhancing unrelated correlations or reducing critical connection strengths. This results in amplification of slight movement or the inability to infer future motion from tiny cues.

To handle the aforementioned challenges, we propose *Dynamic SpatioTemporal Decompose Graph Convolution (DSTD-GC)* to model dynamic spatiotemporal correlations in motion prediction with lightweight spatiotemporal representations. DSTD-GC decomposes spatiotemporal graph modeling into a combination of spatial graph modeling with Dynamic Spatial Graph Convolution (DS-GC) and temporal graph modeling with Dynamic Temporal Graph Convolution (DT-GC). The lightweight dynamic representation capability of DS-GC and DT-GC comes from *constrained dynamic correlation modeling*, which represents the temporal-wise spatial correlations or spatial-wise temporal correlations with the a spatial-shared

*Corresponding author.

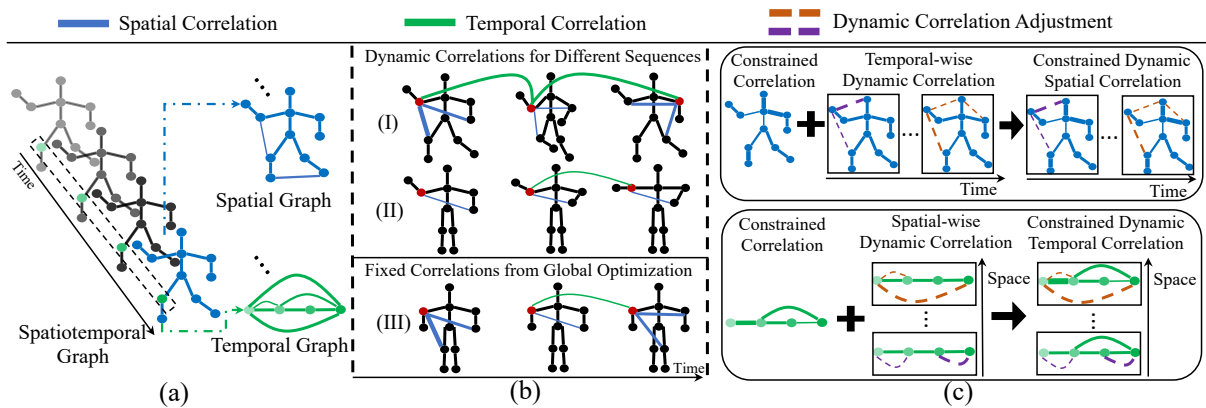


Figure 1: (a) Spatiotemporal graph representation and decomposition. A spatiotemporal graph can be decomposed into multiple spatial graphs and temporal graphs. (b) Dynamic correlation modeling. Correlations vary from different actions, the correlations in running (I) are different from the ones in directing traffic (II). The learned correlations from global optimization (III) can't explicitly capture these variations and introduce correlation amplification or reduction. (c) Constrained dynamic correlation modeling. The spatial correlations consist of a shared constrained correlation and an unshared temporal-wise dynamic correlation. Temporal graph correlations contain shared constrained correlations and unshared spatial-specific correlations.

or temporal-shared correlation and a function to extract spatial-specific or temporal-specific correlation adjustment. This parameter for this representation is only a quarter of previous parameterized decomposition representation [36]. The motivation behind this mechanism is that graph correlations in human motion are both constrained and dynamic. Human motion is generally constrained by shared correlations like joint connections and temporal adjacency. Besides, the correlation strength between certain joints is dynamically enhanced or reduced according to different samples. Figure 1 (c) shows how this mechanism works for a specific sample, the constrained correlation is parameterized as a fixed vanilla spatial or temporal adjacency matrix and is shared by all-time or by all joints. It serves as motion prior and indicates general connections between vertices. The dynamic correlation adjustment is extracted from different samples and complete temporal-wise spatial correlations or spatial-wise temporal correlations. The spatiotemporal graph representation is then reduced to a vanilla adjacency matrix and a correlation adjustment function. In comparison to prior decompositions [36], this representation requires only a fifth of the parameters. Besides, this mechanism also avoids separate correlation modeling and thus reduces optimization difficulty. Furthermore, we analyze different kinds of spatiotemporal graph convolutions in a unified form and theoretically prove that DSTD-GC enhances feature representation by relaxing certain restrictions of spatiotemporal graph convolutions. Based on DSTD-GC, we propose DCTD-GCN which consistently outperforms other state-of-the-art methods in prediction accuracy with the fewest parameters.

In brief, our contributions in this paper can be summarized as follow: (1) We propose Dynamic SpatioTemporal Decompose Graph Convolution, which is the first graph convolution to model dynamic spatiotemporal correlations based on spatiotemporal decomposition in motion prediction; (2) We propose *constrained dynamic modeling* mechanism to efficiently model spatiotemporal correlations,

where prior knowledge is parameterized into light-weight representation and sample-specific correlations are dynamically extracted. (3) We mathematically unify all graph convolutions in spatiotemporal graphs and shows that DSTD-GCN improves representative ability by relaxing limitations of other graph convolutions; (4) We show with extensive experiments that our proposed DSTD-GCN achieves the highest prediction accuracy with the fewest parameters compared with other state-of-the-art baselines.

2 RELATED WORK

In this section, we will first introduce recent advancements in human motion prediction and their limitations in modeling non-grid human motion data. Then we will introduce graph-convolution-based methods which fulfill this gap by treating the non-grid human motion as graphs.

2.1 Human Motion Prediction

Researchers have applied various deep learning techniques in human motion prediction. CNN-based methods mainly treat a human pose as a pseudo-image and stack pose sequence along the channel dimension [20, 23]. RNN-based methods shows their power in modeling temporal motion features and make consistent predictions [8, 20, 21, 25, 26, 30, 33, 35, 37, 38, 42]. GAN-based methods make multiple future predictions based on data pattern similarities and generate realistic results [5, 9, 24, 27]. Transformer-based methods directly model long-range spatial and temporal dependencies [1, 3]. Although these methods make remarkable advancements compared with traditional methods, they can't direct model natural connectivity between body joints. The natural connectivity is crucial for human motion prediction as human motion follows kinetic chains which are constrained by body connections. In order to explicitly model body connections, researchers have looked into graph convolution networks (GCNs).

2.2 Graph Convolution Networks in Motion Prediction

Graph Convolutions are suitable for non-grid and graph-structural data, which has been successfully applied to social network [7], point cloud [34] and traffic prediction [44]. With joints as vertices and bone connections as edges, a human pose can be naturally represented as a graph. Recently, many researchers has applied graph convolutions in motion prediction [5, 6, 22, 25, 28, 29, 36]. Nearly all GCN-based prediction approaches were developed based on Kipt et al. [16], where features are updated in a two-step manner: (1) Feature transformation with a simple linear transformation or a multi-layer perceptron; and (2) Feature aggregation with graph correlations. The graph correlation is the key component that set GCN apart from other deep learning techniques, which explicitly depicts body connections flexibly. For the spatiotemporal graph correlation, all human prediction methods decomposed it into spatial correlations and temporal correlations. Based on decomposed graph correlations, there are two classifications: (1) *Correlation-shared/Correlation-unshared*: this is according to whether graph correlations are shared by joints in temporal-wise spatial graphs or spatial-wise temporal graphs. (2) *Static/Dynamic*: this is based on whether graph correlations are adjusted dynamically during the inference stage.

2.2.1 Correlation-shared/Correlation-unshared Methods. For correlation-shared methods, the spatial correlations are shared across time and temporal correlations are shared across joints. Most of previous works [5, 6, 22, 25, 28, 29] belong to this type. A challenge for these methods is that they can't explicitly model changing spatial relationships in different stages of the action and diverse temporal patterns in different joints. Thus, they generally need to stack many graph convolution layers to model complex spatiotemporal correlations in human motion. For *correlation-unshared methods*, the spatial correlations vary from time and the temporal correlations vary from joints. Sofianos et al. [36] showed that this strategy can explicitly depict joint relationships in spatiotemporal graphs thus explicitly model complex spatiotemporal correlations in human motion with far fewer parameters.

2.2.2 Static/Dynamic Methods. For static methods, graph correlations keep unchanged during inference. Nearly all previous works applied this strategy. Mao et al. [29] and Dang et al. [6] directly learned graph correlations from data, while Li et al. [21] initialize the trainable correlation as a predefined graph. Cui et al. and Liu et al. [5, 25] proposed a semi-constrained graph which consists of prior knowledge and learnt correlations. For *dynamic methods*, graph correlations can be flexible adjusted during inference. To our best knowledge, dynamic graph convolutions are hardly studied in motion prediction. We are the first work to model *dynamic correlation-unshared correlations* in motion prediction.

3 METHODOLOGY

3.1 Preliminaries

3.1.1 Problem Definition. Human motion prediction is to predict L future human pose frames with K historical observations. As a human pose is represented by J joints with D -dimensional spatial

information, we denote the human pose at time t as $X_t \in \mathbb{R}^{J \times D}$. The historical observations are formulated as $X_{1:K} = \{X_1, \dots, X_K\}$. Our goal is to predict the future human motion $\hat{X}_{K+1:K+L} = \{\hat{X}_{K+1}, \dots, \hat{X}_{K+L}\}$ where the corresponding ground truth is denoted as $X_{K+1:K+L} = \{X_{K+1}, \dots, X_{K+L}\}$.

3.1.2 Notations. We formally define spatiotemporal graph convolution and spatiotemporal decomposition used in our paper.

Spatiotemporal Graph Representation. As shown in Figure 1 (a), a human motion sequence with T frames is presented as a spatiotemporal graph $\mathcal{G}^{st} = (\mathcal{V}^{st}, \mathcal{E}^{st})$, where $\mathcal{V}^{st} \in \mathbb{R}^{JT}$ is the set of all joints across time and \mathcal{E}^{st} is the spatiotemporal edge set. $A^{JT \times JT}$ is the spatiotemporal adjacency matrix, which represent correlations between vertices in the graph. Due to the high computation difficulty of the spatiotemporal adjacency matrix, we further decompose a spatiotemporal graph into a unique pair of T spatial graph across time and J temporal graphs across joints. The spatial graphs are denoted as $\mathcal{G}^s = (\mathcal{V}^s, \mathcal{E}^s)$ where $\mathcal{V}^s \in \mathbb{R}^{T \times J}$ is the joint vertex set. \mathcal{E}^s is the spatial edge set and is formulated as a spatial adjacency matrix¹ $A^s \in \mathbb{R}^{T \times J \times J}$. When N graphs share the same spatial correlations, the spatial adjacency matrix is degraded into vanilla form and can be represented by a matrix from $\mathbb{R}^{J \times J}$. Similarly, the temporal graphs are denoted as $\mathcal{G}^t = (\mathcal{V}^t, \mathcal{E}^t)$ where $\mathcal{V}^t \in \mathbb{R}^{J \times T}$ is the trajectory vertex set. \mathcal{E}^t is the temporal edge set and is formulated as a temporal adjacency matrix $A^t \in \mathbb{R}^{J \times T \times T}$.

Spatiotemporal-equivalence. With the definition of spatial and temporal graphs, we now define equivalent operation on these two graphs. The spatiotemporal-equivalence is defined between two operations on spatial graphs and corresponding temporal graphs. Formally, function \mathcal{F}^s on \mathcal{G}^s and function \mathcal{F}^t on corresponding \mathcal{G}^t are spatiotemporal-equivalent if and only if \mathcal{F}^s is equivalent to \mathcal{F}^t after switching all operations for time dimension and for space dimension and vice versa. For a function \mathcal{F}^s on \mathcal{G}^s , there is strictly one spatiotemporal-equivalent \mathcal{F}^t on corresponding \mathcal{G}^t .

3.1.3 Spatiotemporal Decompose Graph Convolutions. We introduce different graph convolutions with the example of the feature updating process for the joint q of time n . For a typical spatiotemporal graph convolution (ST-GC) layer, the whole process is formulated as:

$$y_{qn} = \sum_p^J \sum_m^T a_{(pm)(qn)}^{st} x_{pm} W, \quad (1)$$

where $x_{pm} \in \mathbb{R}^C$ is the input feature, $y_{qn} \in \mathbb{R}^C$ is the output feature, and $W \in \mathbb{R}^{C \times C'}$ is a trainable parameter for feature transformation.

With the graph decomposition introduced above, we define two graph convolutions: spatial graph convolution (S-GC) and temporal graph convolution (T-GC). The detailed formulations are described as:

$$x_{qn}^s = \sum_p^J a_{npq}^s x_{pn} W, \quad (2)$$

$$x_{qn}^t = \sum_m^T a_{qmn}^t x_{qm} W. \quad (3)$$

¹We denote both second and third order tensor as matrix in this paper for clarity.

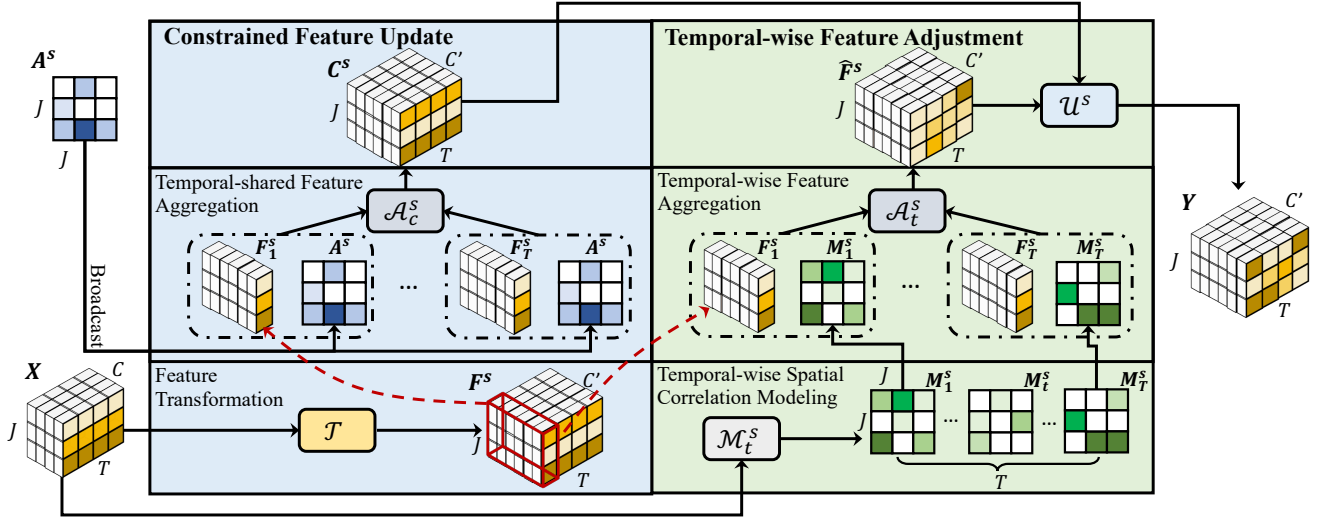


Figure 2: The framework of Dynamic Spatial Graph Convolution (DS-GC). Constrained feature update aggregates motion representation with temporal-shared correlations. Temporal-wise Feature Adjustment obtains motion representations with temporal-specific correlations, where the correlations are obtained with temporal-wise correlation modeling. Eventually, the output feature is obtained by constrained correlations with temporal-wise adjustment.

Specifically, the S-GC models temporal-wise spatial correlations, while T-GC models spatial-wise temporal correlations. We then propose *SpatioTemporal Decompose Graph Convolution (STD-GC)* by alternatively stacking a S-GC (Equation 2) and a T-GC (Equation 3):

$$y_{qn} = \sum_m^T a_{qmn}^t \left(\sum_p^J a_{npq}^s x_{pm} W_1 \right) W_2. \quad (4)$$

STD-GC decomposes ST-GC on a spatiotemporal graph into S-GC on corresponding spatial graphs and T-GC on corresponding temporal graphs, spatiotemporal feature modeling is accomplished by consecutive stacking of the two graph convolutions. The spatiotemporal modeling capability is invariant to the stacking order of S-GC and T-GC. Besides, STD-GC is equivalent to STS-GC [36]. We will demonstrate all of these with experiments in Section 4.3.

In static methods, a_{npq}^s and a_{qmn}^t are set based on prior knowledge or defined as trainable parameters. In dynamic methods, a_{npq}^s and a_{qmn}^t are generated by model according to input samples.

3.2 Constrained Dynamic Correlation Modeling

The correlations between joints are both constrained and dynamic. For one thing, the correlations between joints are constrained by the inherent human body structure and learned motion prior. For another, these constrained correlations are varied from different motion sequences. To show these two aspects, we utilize correlations of the elbow joint in the running scenarios as an example. On the one hand, The elbow movement generally follows motion chain of human body and shared trajectory pattern, this constraints represented by shared spatiotemporal correlations. On the other hand, the spatial correlations between the elbow joint and the knee joint is generally stronger than the correlation in directing traffic

scenarios, and temporal correlations are more periodic than the ones in directing traffic.

Inspired by this, we can represent spatiotemporal graph correlations with lightweight vanilla spatial and temporal correlations and a function to extract dynamic unshared correlations. Therefore, we introduce *Dynamic SpatioTemporal Decompose Graph Convolution (DSTD-GC)*. DSTD-GC consists of a pair of spatiotemporal-equivalent graph convolution Dynamic Spatial Graph Convolutions (DS-GC) and Dynamic Temporal Graph Convolutions (DT-GC). Specifically, DS-GC models dynamic temporal-specific spatial correlations, while DT-GC models dynamic spatial-specific temporal correlations. By combing these two graph convolutions, DSTD-GC can model dynamic spatiotemporal correlations. We now look into DS-GC and DT-GC in detail. For clarity, We only introduce DS-GC, and its spatiotemporal-equivalent counterpart DT-GC can be deduced naturally. The general framework of DS-GC is illustrated in Figure 2. Specifically, DS-GC consists of two parts: (1) Constrained feature update with shared vanilla correlations; (2) Temporal-wise feature adjustment. The first part updates motion features with shared constrained constraints, while the last part completes feature representations by modeling dynamic temporal-wise spatial correlations from different samples. Specifically, A DS-GC layer receives motion feature $X \in \mathbb{R}^{J \times T \times C}$ and shared constrained spatial correlation $A^s \in \mathbb{R}^{J \times J}$ as inputs, and then outputs $Y \in \mathbb{R}^{J \times T \times C}$.

3.2.1 Constrained Feature Update. As shown in the blue block of Figure 2, constrained feature update is no different from vanilla S-GC where spatial correlations are shared across time. Specifically, feature transformation is accomplished by transformation function \mathcal{T} . Here we set the function as a linear transformation function for clarity while other functions like a multi-layer perceptron can also

be adopted. The function is defined as:

$$F^s = \mathcal{T}(X) = XW, \quad (5)$$

where $F^{(s)} \in \mathbb{R}^{J \times T \times C'}$ is the high-level representations. After feature transformation, features are aggregated across time with aggregation function \mathcal{A}_t^s to obtain updated constrained feature C^s . The whole process to obtain in constrained feature update is formulated as:

$$C^s = \mathcal{A}_t^s(F^s, A^s) = [F^s_{:,1} A^s ||_t \cdots ||_t F^s_{:,T} A^s], \quad (6)$$

where $||_t$ is concatenation function along the time dimension. A^s is vanilla spatial correlations and guide feature aggregation with the broadcast mechanism.

3.2.2 Temporal-wise Feature Adjustment. The temporal-wise feature adjustment is shown in the green part of Figure 2. Here temporal-specific spatial correlations $M^s \in \mathbb{R}^{T \times J \times J}$ is inferred from the input sample to capture dynamic temporal-wise spatial correlations. Specifically, M^s is extracted by the temporal-wise spatial correlation modeling function \mathcal{M}_t^s , which traverses every pair of joints to extract correlations between them. This function for a joint pair (j_x, j_y) is formulated as:

$$M^s = \mathcal{M}_t^s(f_x^s, f_y^s) = \text{MLP}_1(\theta(f_x^s) ||_s^p \phi(f_y^s)), \quad (7)$$

where (f_x^s, f_y^s) are corresponding transformed representation of the joint pair and $||_s^p$ is pair-wise concatenation for joints. θ and ϕ are two linear transformation functions, which project the joint features into low-dimensional representations to reduce computational cost. MLP_1 is a multi-layer perceptron, we utilize MLP because it is capable of modeling complex spatial correlations. Note that M^s is not required to be symmetric, this benefits correlation modeling by increasing analysis flexibility and enhancing representative ability. Besides, M^s is also varied from different input samples.

Given the temporal-specific spatial correlations M^s from input samples, we aggregate features with temporal-wise aggregation function \mathcal{A}_t^s , where aggregated feature $\hat{F}^s \in \mathbb{R}^{J \times T \times C'}$ is obtained by:

$$\hat{F}^s = \mathcal{A}_t^s(F^s, M^s) = [F^s_{:,1} M^s ||_t \cdots ||_t F^s_{:,T} M^s]. \quad (8)$$

Finally, the output representation with dynamic temporal-wise adjustment, $H^{(l+1)}$, is obtained by adjusting constrained representation C^s with temporal-specific representation \hat{F}^s :

$$E^s = \mathcal{U}_t^s(C^s, \hat{F}^s) = C^s + \alpha \cdot \hat{F}^s, \quad (9)$$

where α is a learnable parameter to control the adjustment intensity. Based on these functions, DS-GC can be formulated as:

$$Y = \mathcal{U}^s(A_c^s(\mathcal{T}(X), A^s), A_t^s(\mathcal{T}(X), \mathcal{M}_t^s(X))). \quad (10)$$

Since DT-GC is spatiotemporal-equivalent to DS-GC, DT-GC can be directly obtained by replacing all operations in DS-GC with their spatiotemporal-equivalent counterpart.

3.2.3 Discussion. Compared with STS-GC/STD-GC, DSTD-GC contains three advantages: (1) *Parameter-saving*: STS-GC learn a spatial adjacency matrix A^s and a temporal adjacency matrix A^t , where the space complexity is $O(JT^2 + J^2T)$. Conversely, DSTD-GC saves a great many parameters by learning the previous two adjacency matrices in vanilla form with few extra operations, where the space

complexity is $O(T^2 + J^2)$. As the joint number is always proportional to the sequence length, The space complexity for STS-GC is $O(T^3)$ while the one DSTD-GC is only with $O(T^2)$. (2) *Joint optimization*: DSTD-GC learns shared graph correlations and dynamic correlation variations between different times or different joints. This mechanism has less optimization difficulty than learning optimal spatial correlation at different times or temporal correlations in different joints separately. (3) *Dynamic*: DSTD-GC adopts an adjustment strategy that can better model dynamic spatiotemporal correlations in different motion inputs.

3.3 Analysis of Graph Convolutions on Spatiotemporal Graphs

In this section, we analyze the representation capability of different graph convolutions on spatiotemporal graphs in human motion prediction by reformulating them into a unified form. Since there is no work on directly depicting correlations in spatiotemporal graphs, we first introduce the constraint of the spatiotemporal graph decomposition, then evaluate different graph convolutions based on their spatial and temporal modeling capability.

By comparing ST-GC (Equation 1) and STD-GC (Equation 4), the spatiotemporal correlations can be represented by a combination of spatial correlations and temporal correlations with the following constraints:

Constraint 1: $a_{(pm)(qn)}^{st(i)}$ is equal to the product of $a_{npq}^{s(i)}$ and $a_{qmn}^{t(i)}$.

Note that here $a_{(pm)(qn)}^{st(i)}$ is the spatiotemporal correlation strength, $a_{npq}^{s(i)}$ is corresponding spatial correlation strength, and $a_{qmn}^{t(i)}$ is corresponding temporal correlation strength.

Based on the decomposition constraint, we further reformulate decomposed ST-GC from the spatial graph's view and the temporal graph's view can be defined as:

$$y_{qn}^{(i)} = \sum_p a_{npq}^{s(i)} \sum_m x_{pm}^{(i)} (a_{qmn}^{t(i)} W) = \sum_p a_{npq}^{s(i)} \sum_m x_{pm}^{(i)} R_{qmn}^{t(i)}, \quad (11)$$

$$y_{qn}^{(i)} = \sum_m a_{qmn}^{t(i)} \sum_p x_{pm}^{(i)} (a_{npq}^{s(i)} W) = \sum_m a_{qmn}^{t(i)} \sum_p x_{pm}^{(i)} R_{npq}^{s(i)}, \quad (12)$$

where $a_{npq}^{s(i)}$ and $a_{qmn}^{t(i)}$ are the spatial correlation weight and temporal correlation weight for the input sample. Furthermore, we combine correlation strength and feature transformation weights into a generalized weight matrix $R_{***}^{*(i)}$. Therefore, the feature updating process consists of feature transformation with the generalized weight matrix and feature aggregation with temporal-wise spatial or spatial-wise temporal correlations. With these two formulations, we then analyze different graph convolutions based on the spatial and temporal correlations for feature aggregation.

3.3.1 Static Correlation-shared Graph Convolutions. Most recent works [5, 6, 22, 28, 29, 43] adopted correlation-shared graph convolution, where joint vertices from all times share one spatial correlation and trajectory vertices for all joints share one temporal correlation. The whole graph convolution process can be formulated as:

$$y_{qn}^{(i)} = \sum_p \sum_m a_{pq}^s a_{mn}^t x_{pm}^{(i)} W, \quad (13)$$

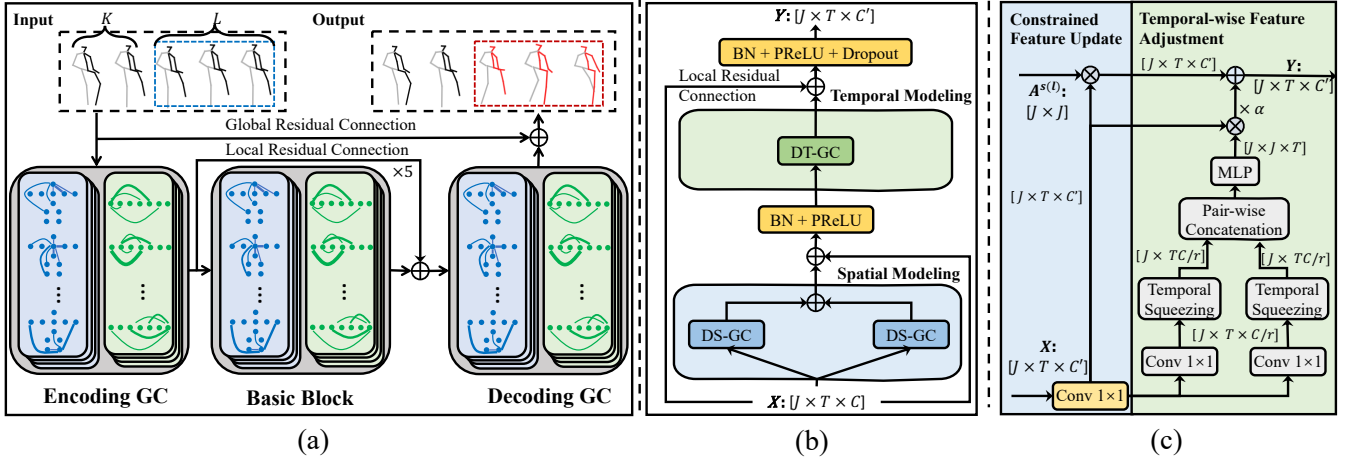


Figure 3: (a) Problem Reformulation and Prediction Framework. Human poses in the blue dashed box are duplicate inputs, while poses in the red box are target predictions. (b) The basic block of DSTD-GCN. The DS-GCN aims to adjust self-loop constrain, natural connection constraint and semantic connection constraint separately with three DS-GCs, while DT-GCN refines self-loop constraint and context connections constraint simultaneously with two DT-GCs. (c) Implementation of DS-GC. The boxes with different colors indicate different functions.

Table 1: Comparison of different graph convolutions.

Correlations		Constraints					Methods	Params.	MPJPE						
Unshared	Dynamic	1	2	3	4	5			80	160	320	400	560	1000	Average
✓	✗	✓	✓				ST-GC (3.1.2)	5.44M	9.27	16.87	31.67	38.98	52.29	80.23	38.22
✗	✗	✓	✓	✓			VST-GC (3.1.2)	0.10M	9.08	17.06	33.67	41.75	56.19	87.01	40.79
✗	✗	✓	✓	✓			FC-GC [29]	0.29M	13.13	24.49	44.91	53.85	69.65	99.00	50.84
✓	✗	✓	✓	✓			STS-GC [36]	0.45M	8.95	16.40	31.35	38.64	52.11	80.27	38.29
✓	✗	✓	✓	✓			TSD-GC	0.46M	8.53	15.83	31.03	38.79	53.16	82.17	38.25
✓	✗	✓	✓	✓			STD-GC	0.46M	8.78	16.25	31.12	38.41	52.15	80.93	37.85
✓	✓	✓		✓	✓		DTSD-GC	0.13M	8.43	15.08	30.25	37.68	51.03	81.02	37.08
✓	✓	✓		✓	✓		DSTD-GC	0.13M	8.10	15.16	29.88	37.01	50.24	79.67	36.68

$$y_{qn}^{(i)} = \sum_p^J a_{pq}^s \sum_m^T x_{pm}^{(i)} (a_{mn}^t W), \quad (14)$$

$$y_{qn}^{(i)} = \sum_m^T a_{mn}^t \sum_p^J x_{pm}^{(i)} (a_{pq}^s W). \quad (15)$$

Note that a_{pq}^s is temporal-shared spatial correlation strength and a_{mn}^t is spatial-shared spatial correlation strength, they are respectively from the vanilla form of the spatial adjacency matrix and the temporal adjacency matrix. Equation 14 and 15 are the reformulations of Equation 13 in spatial graph's view and temporal graph's view respectively. Besides, the two correlations are stay unchanged across input samples. Therefore, the static spatial/temporal graph convolutions are subject to following constraints:

Constraint 2: $a_{m_1 p q}^{s(i)}$ and $a_{m_2 p q}^{s(i)}$ are forced to be the same, $a_{q_1 m n}^{t(i)}$ and $a_{q_2 m n}^{t(i)}$ are forced to be the same.

Constraint 3: $a_{m p q}^{s(i_1)}$ and $a_{m p q}^{s(i_2)}$ are forced to be the same, $a_{q m n}^{t(i_1)}$ and $a_{q m n}^{t(i_2)}$ are forced to be the same.

Note that i_1, i_2 are different input sample indices, m_1, m_2 are indices of different joints and q_1, q_2 indicate indices of different time.

3.3.2 Static Correlation-unshared Graph Convolutions. The only difference between static spatial/temporal graph convolutions and static spatiotemporal graph convolutions is that the static spatiotemporal ones adopt unshared spatial and temporal correlations. Static spatiotemporal graph convolutions can be formulated as:

$$y_{qn}^{(i)} = \sum_p^J \sum_m^T a_{npq}^s a_{qmn}^t x_{pm}^{(i)} W, \quad (16)$$

$$y_{qn}^{(i)} = \sum_p^J a_{npq}^s \sum_m^T x_{pm}^{(i)} (a_{qmn}^t W), \quad (17)$$

$$y_{qn}^{(i)} = \sum_m^T a_{qmn}^t \sum_p^J x_{pm}^{(i)} (a_{npq}^s W). \quad (18)$$

Note that a_{npq}^s is temporal-wise spatial correlation strength and a_{qmn}^t is spatial-shared spatial correlation strength, they are respectively from the spatial adjacency matrix and the temporal adjacency matrix. With the two unshared correlations, static spatiotemporal graph convolutions capture evolving spatial relationships between joints at different action stages and diverse temporal relationships for different body parts. Thus, they generally outperform spatial/temporal graph convolutions. However, these correlations are optimized across all data and may not be optimized for individual action sequences. From the formula's view, static spatiotemporal graph convolutions still suffer from *Constraint 2* but relax *Constraint 1* into the following constraint:

Constraint 4: $a_{m_1pq}^{s(i)}$ and $a_{m_2pq}^{s(i)}$ differ by a scaling factor, $a_{q_1mn}^{t(i)}$ and $a_{q_2mn}^{t(i)}$ differ by a scaling factor.

3.3.3 Dynamic Correlation-unshared Graph Convolutions. In comparison to static spatiotemporal graph convolutions, the dynamic ones dynamically infer correlations between vertices and thus have a higher capacity for representation. The formulation of dynamic spatiotemporal graph convolutions is:

$$y_{qn}^{(i)} = \sum_p \sum_m^T a_{npq}^{s(i)} a_{qmn}^{t(i)} x_{pm}^{(i)} W, \quad (19)$$

$$y_{qn}^{(i)} = \sum_p a_{npq}^{s(i)} \sum_m^T x_{pm}^{(i)} (a_{qmn}^{t(i)} W), \quad (20)$$

$$y_{qn}^{(i)} = \sum_m^T a_{qmn}^{t(i)} \sum_p x_{pm}^{(i)} (a_{npq}^{s(i)} W). \quad (21)$$

Note that both $a_{npq}^{s(i)}$ and $a_{qmn}^{t(i)}$ are adjustable to the input sample i . Based on these formulations, dynamic spatiotemporal graph convolutions relax both *Constraint 2* and *3*. Concretely, they relax *Constraint 2* into *Constraint 4* and relax *Constraint 3* into the following constraint:

Constraint 5: $a_{npq}^{s(i_1)}$ and $a_{npq}^{s(i_2)}$ differ by a scaling factor, $a_{qmn}^{t(i_1)}$ and $a_{qmn}^{t(i_2)}$ differ by a scaling factor.

We summarize different types of graph convolutions on spatiotemporal graphs in table 1. It can be seen that dynamic spatiotemporal graph convolution is the least constrained spatiotemporal decompose graph convolution. Our DSTD-GC belongs to dynamic spatiotemporal graph convolution. Thus, DSTD-GC has a stronger representation capability than previous graph convolutions [29, 36]. We can reformulate DSTD-GC into Equation 19, Equation 20 and Equation 21 respectively, as we will shown in supplementary materials.

3.4 Model Architecture

Based on DSTD-GC, we build a light-weight and powerful model DSTD-GCN, which is based on the prediction framework proposed by [29]. We will first introduce the prediction framework, then introduce the architecture of our proposed DSTD-GCN.

3.4.1 Prediction Framework. We duplicate the last input human pose for L times and formulate a new input motion sequence $X_{1:K+L}$. Then the original prediction task is reformulated into predicting the residual motion sequence between $\tilde{X}_{1:K+L}$ and corresponding

ground truth $X_{1:K+L}$. Based on the problem reformulation, the prediction framework is proposed as shown in Figure 3 (a). The effectiveness of this framework is illustrated in recent studies [5, 6, 29]. With this framework, we can model the input and output human poses as a whole sequence and model joint spatiotemporal correlations, while the previous framework [21, 36] only models spatiotemporal correlations for the input frames. We will use this framework to build our model and compare different kinds of graph convolutions.

3.4.2 Model Architecture. The entire network contains five basic blocks. The basic block of DSTD-GCN is shown in Figure 3 (b), which contains a DS-GCN for spatial modeling and a DT-GCN for temporal modeling. The number of channels in the basic block is set as 64. The DS-GCN consists of three parallel DS-GCs, while DT-GCN contains two parallel DT-GCs. Due to the spatiotemporal-equivalence, we only introduce a detailed implementation of DS-GC. Specifically, the modeling function \mathcal{M}_i^s receives inputs $X \in \mathbb{R}^{T \times C}$. We squeeze the temporal dimension into the channel dimension and direct extract temporal-wise spatial correlations with a linear transformation. Since the computation for direct transformation from $T \times C$ to T is high. We utilize two linear transformation functions θ and ϕ to transform X into a neatly compact representation, then preforms a temporal squeeze operation. After, a pair-wise concatenation and *MLP* are adapted to extract temporal-wise spatial correlations. The final result is a combination of constrained and dynamic correlations. We further consider prior knowledge connections and initialize constrained spatial correlations as self-loop, natural connections and semantic connections such as relationships between two hands, respectively. The initial constrained temporal correlations are set as connections to oneself and its context frames.

4 EXPERIMENTS

To evaluate the effectiveness of our proposed model, we run experiments on two standard benchmark motion capture datasets, which include Human3.6M [13] and the CMU Mocap dataset. Experiments are designed to answer the following research questions: (1) *what is the performance of DSTD-GC as compared to other Graph Convolution?* (2) *what is the performance of our proposed DSTD-GCN as compared to other state-of-art motion prediction methods?* (3) *what is the influence of different components and what insights and findings can we learn from the experimental results?*

4.1 Datasets Settings

We evaluate our proposed DSTD-GCN on two large-scale benchmark baselines.

Human3.6M. Human3.6M [13] is considered to be a wide-spread benchmark dataset for evaluating motion prediction. It consists of 15 complex actions performed by 7 actors, including aperiodic ones (e.g., smoking) and periodic ones (e.g., running). Following the data preprocessing procedure of [6, 29, 30], the original data in exponential mapping format is transformed into 3D joint coordinate space and a single pose is represented by 32 body joints. Besides, each data sequence is down-sampled to 25 FPS. The data from S5 and S11 are used as test and validation datasets, while the rest of the 5 subjects are for training.

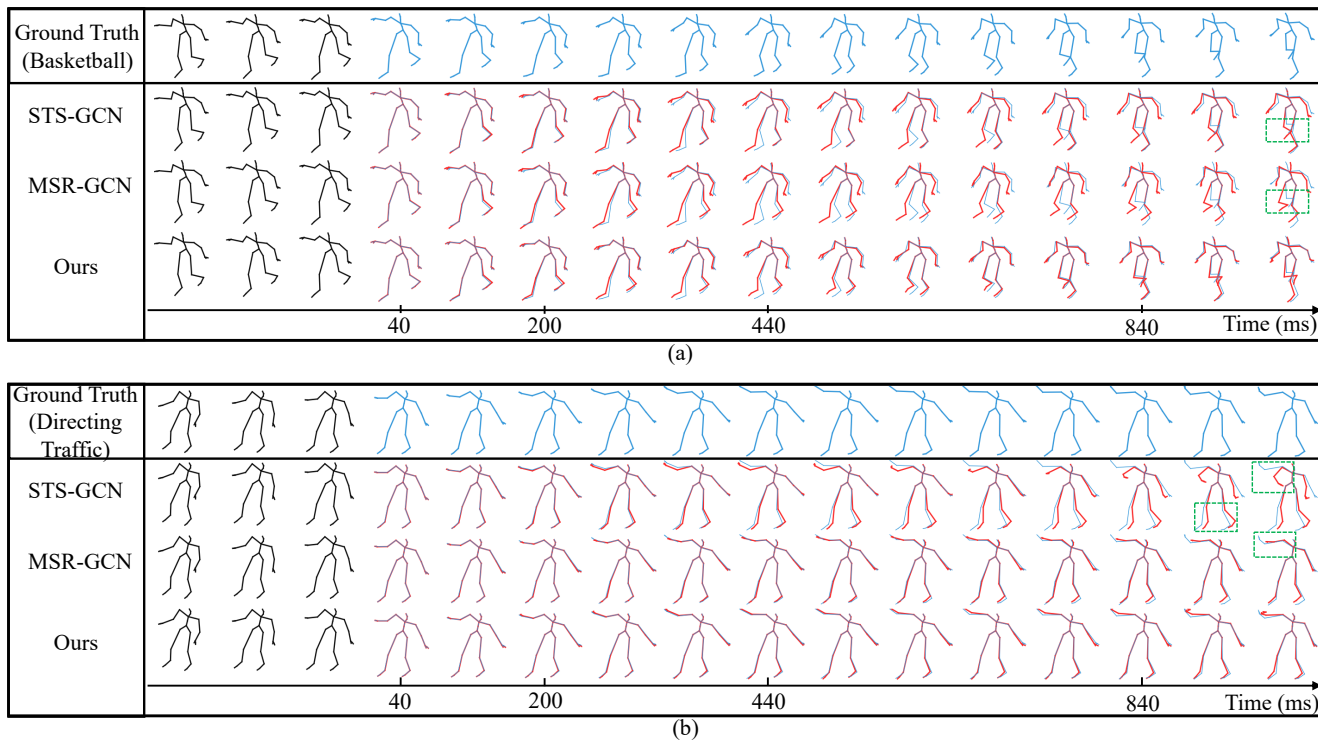


Figure 4: Visualization of predicted results of state-of-the-art methods on two action examples on CMU-Mocap dataset. The black, blue and red poses indicate inputs, ground truths and predictions respectively. (a) Basketball. (b) Directing Traffic.

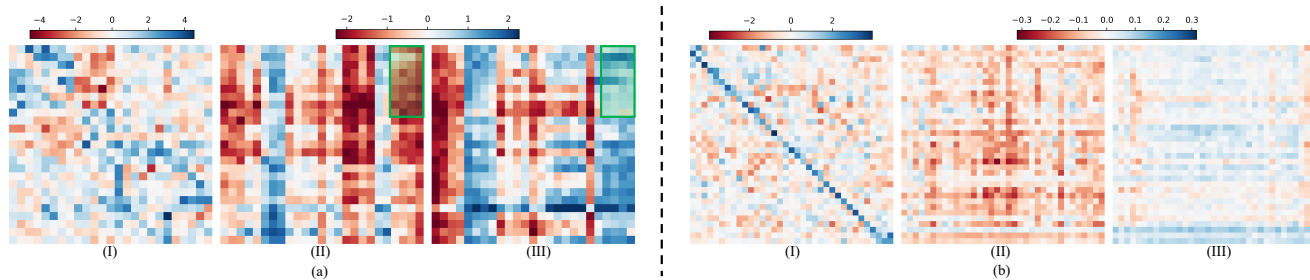


Figure 5: Visualization of spatial and temporal correlation. (a) Spatial correlation from a predicted human pose frame. (b) Temporal correlation from a joint trajectory. (I) Constrained correlation. (II) and (III) are dynamic correlation adjustments of a pose frame or a joint trajectory for two different action sequences.

CMU Mocap. CMU Mocap dataset² contains 8 actions. All action sequences are also down-sampled to 25 FPS and each pose is represented by 38 body joints. The rest pre-processing procedure is the same as Human3.6M. Following the experiment literature of [20], we adopt the same train/test split strategy.

Test Set Size and Sample Length. Most previous works only evaluated their models with 8 sequences for each action [5, 23, 29, 30], researchers argued that this strategy is biased and can't fully evaluate the model's performance [6, 28]. Therefore, we use the full test

set following Dang *et al.* [6]. Besides, We set the input length as 10 and output length as 25 following Dang *et al.*

4.2 Comparison Settings

4.2.1 Metrics. The Mean Per Joint Position Error (MPJPE) is a standard evaluation metric used in previous studies [6, 20, 30]. With the predicted motion sequence $\hat{X}_{K+1:K+L}$ and corresponding ground truth $X_{K+1:K+L}$, the MPJPE loss is defined as

$$\mathcal{L}_{MPJPE} = \frac{1}{J \times L} \sum_{t=K+1}^{K+L} \sum_{j=1}^J \|\hat{p}_{j,t} - p_{j,t}\|_2, \quad (22)$$

²<http://mocap.cs.cmu.edu/>

where $\tilde{p}_{j,t} \in \mathbb{R}^D$ is the predicted j th joint position in frame t , while $p_{i,t} \in \mathbb{R}^D$ is the corresponding ground truth.

4.2.2 Implementation Details. We conduct all experiments on one RTX 3080 Ti GPU with the Pytorch framework [32]. For the comparison baseline and DSTD-GCN, we set the dropout rate as 0.1 and chose PReLU [11] as the activation function. Besides, all the models were trained with Adam optimizer [15] with an initial learning rate of $3e-3$, which decays by 0.9 for every 5 epochs. We also use MPJPE as the loss function and set the batch size as 32.

4.3 RQ1: Comparison with other GCs

In order to verify our DSTD-GC’s effectiveness, we compare parameters, and performance of DSTD-GC against other graph convolutions in Table 1. Specifically, TSD-GC and DSTD-GC differs from STD-GC and DSTD-GC in the order of spatial graph convolution and temporal graph convolution. For a fair comparison, we keep the prediction framework unchanged and merely replace graph convolutions. We also exchange linear transformation to *MLP* to make the number of feature transformations the same and utilized a random initialized adjacency matrix across models. From Table 1, we observe that (1) Overall, spatiotemporal methods outperform spatial/temporal methods, and dynamic methods outperform static methods, highlighting the importance of spatiotemporal graph modeling and dynamic correlations; (2) STD-GC, STS-GC and ST-GC perform similarly, but ST-GC has far more parameters than the other two graph convolutions, demonstrating the critical role of spatiotemporal decomposition; (3) STD-GC slightly outperforms STS-GC, demonstrating the effectiveness of further decomposition of spatiotemporal modeling; (4) DSTD-GC outperforms STD-GC by 1.17 with 28.3% parameters, proving that our constrained dynamic modeling strategy is effective to model spatiotemporal correlations in human motions. (5). STD-GC and TSD-GC, DSTD-GC and DTSD-GC performs similarly, indicating that the order of spatial and temporal relationship modeling have little effect for spatiotemporal correlation modeling in the decomposition scenario.

4.4 RQ2: Comparison with the State-of-the-art

To evaluate the performance of DSTD-GCN, we present the quantitative and qualitative results on Human3.6M and CMU Mocap datasets. We first introduce the compared baselines and then introduce DSTD-GCN’s performance. Following literature from previous works [6, 29], we divide the results into short-term (< 500 msecs) and long-term (> 500 msecs) predictions.

4.4.1 Baselines. To evaluate the effectiveness of DSTD-GCN, we select six state-of-the-art baselines, including RNN-based model (Residual sup [30]), CNN-based model (Traj-CNN [23]) and GCN-based model (FC-GCN [29], DMGNN [21] and MSR-GCN [6] and STS-GCN [36]). For GCN-based models, FC-GCN, DMGNN, and MSR-GCN belong to the static spatial/temporal method, and STS-GCN³ is the only static spatiotemporal method. For the graph correlations, DMGNN adopts fixed correlations from body connections, while the other three GCN-based methods initialize the adjacency matrix randomly and then optimize it with back-propagation.

³We utilized the model from RQ1

Among all baseline methods, FC-GCN, Traj-CNN, MSR-GCN, STS-GCN, and our methods adopt the prediction framework shown in Figure 3 (a).

4.4.2 Results. The detail quantitative comparisons for both short-term and long-term prediction results are presented in Table 2 and Table 3. Besides, we also present the average results of selected frames, and model parameters in Table 4. More intuitive comparisons are shown in Figure 6. Apparently, methods with the prediction framework make more accurate predictions with fewer parameters. Besides, GCN-based methods generally outperform the RNN-based method (Residual Sup.) and CNN-based methods (Traj-CNN). With dynamic spatiotemporal correlation modeling, our methods achieve the best prediction accuracy with the fewest parameters. It is also worth noting that the parameter number of our method is half of the most lightweight model STS-GCN. Besides, our model only cost 3% parameters of the best baseline MSR-GCN on the CMU Mocap dataset. Moreover, we show two examples of the predicted poses for different methods in Figure 4. In the basketball scenario, body joints move drastically. Under these circumstances, spatiotemporal methods generally work better than spatial/temporal ones as spatiotemporal methods explicitly model each joint’s spatiotemporal correlations and can infer large movement from tiny motion cues. Here, both STS-GCN and our method capture the backward trend of the right feet. However, statically modeling spatiotemporal correlations may disturb individual motion prediction, especially in some static action scenarios. As we see in directing traffic scenario, most joints stay still. Here, STS-GCN misamplify the motion of the right arm and infers feet movement mistakenly. With the constrained dynamic correlation modeling strategy, our methods can dynamically thus make more accurate predictions under different scenarios.

4.4.3 Visualization of Constrained Dynamic Correlations. To better understand why our method takes effect, we visualize the spatial and temporal correlations from the two examples in Figure 4. The sample correlations are shown Figure 5. We obtain two observations: (1) The constrained correlation strength is larger than the adjusted one, demonstrating that the basics of motion prediction come from static correlation. (2) Dynamic correlation adjustments vary from different input samples. As shown in Figure 5 (a), (II) and (III) indicate dynamic spatial correlation adjustments of basketball and directing traffic. Compared with the adjustment strength from the right arm to the feet (green box), we find the corresponding correlations is enhanced in basketball and reduced in directing traffic. These adjustments are reasonable because arms and feet collaborate intensively in the basketball example but feet is still and unrelated to the movement of the right arm in the directing traffic case. Moreover, we also present temporal correlation adjustments from a right foot joint in Figure 5 (b), we find the adjustment strengths in generally stronger in the basketball case. As the right foot move backward in the basketball example, it correlate to other vertices in the trajectory more intensively. With this visualization, we observe that our proposed constrained dynamic correlation modeling strategy can generate sample-specific correlation thus make more accurate prediction.

Table 2: Comparisons of predictions on Human3.6M. The best results are highlighted in bold, while the second best results are shown in underline.

Action	Walking						Eating						Smoking					
Millisecond (ms)	80	160	320	400	560	1000	80	160	320	400	560	1000	80	160	320	400	560	1000
Residual sup. [30]	24.13	38.59	55.09	59.26	65.14	82.04	18.64	30.38	47.97	54.84	67.80	105.56	18.06	29.63	45.80	52.56	64.25	91.95
DMGNN [21]	15.52	27.42	46.20	54.96	58.86	83.74	10.34	19.84	37.60	46.66	57.95	86.55	9.94	18.90	35.02	42.82	53.23	77.76
FC-GCN [29]	12.29	23.03	39.77	46.12	54.05	59.75	8.36	16.90	33.19	40.70	53.39	77.75	7.94	16.24	31.90	38.90	50.74	72.62
Traj-CNN [23]	<u>11.91</u>	<u>22.54</u>	38.66	45.71	54.49	62.01	8.41	<u>16.56</u>	<u>32.44</u>	<u>39.82</u>	53.47	78.40	8.41	16.17	<u>31.06</u>	<u>37.58</u>	<u>49.30</u>	72.31
STS-GCN [36]	11.98	22.96	41.53	48.47	56.62	62.69	<u>7.90</u>	16.79	33.38	40.74	53.10	<u>76.73</u>	<u>7.48</u>	<u>15.69</u>	31.33	38.45	50.67	73.10
MSR-GCN [6]	12.16	22.65	38.64	<u>45.24</u>	<u>52.72</u>	63.04	8.39	17.05	33.03	40.43	<u>52.54</u>	77.11	8.02	16.27	31.32	38.15	49.45	<u>71.64</u>
Ours	11.05	22.35	38.81	45.19	52.70	<u>59.76</u>	6.95	15.51	31.74	39.19	51.86	76.19	6.64	14.75	29.78	36.67	48.09	71.16
Action	Directions						Greetings						Phoning					
Millisecond (ms)	80	160	320	400	560	1000	80	160	320	400	560	1000	80	160	320	400	560	1000
Residual sup. [30]	21.93	37.38	61.51	71.86	88.09	122.08	35.28	61.98	99.06	111.04	127.44	160.59	21.05	35.49	57.89	67.26	83.74	130.34
DMGNN [21]	10.77	22.81	46.70	57.35	73.51	104.37	20.45	41.13	78.99	94.34	114.68	148.75	12.35	24.25	47.22	58.27	73.62	113.05
FC-GCN [29]	8.97	19.87	43.35	<u>53.74</u>	71.01	101.79	18.65	38.68	77.74	93.39	114.43	148.69	10.24	21.02	42.54	52.30	69.56	104.50
Traj-CNN [23]	8.69	19.29	43.57	54.36	74.56	109.42	15.81	35.12	73.56	<u>88.89</u>	<u>110.78</u>	149.55	10.14	20.52	41.95	51.86	69.29	104.41
STS-GCN [36]	<u>7.82</u>	<u>18.72</u>	<u>42.58</u>	53.25	70.95	102.10	<u>15.33</u>	<u>35.01</u>	<u>73.44</u>	89.08	112.19	<u>143.91</u>	<u>9.54</u>	<u>20.35</u>	41.55	<u>51.07</u>	68.32	<u>103.69</u>
MSR-GCN [6]	8.61	19.65	43.28	53.82	71.18	<u>100.59</u>	16.48	36.95	77.32	93.38	116.26	147.26	10.10	20.74	<u>41.51</u>	51.26	<u>68.29</u>	104.27
Ours	6.86	17.39	40.96	51.67	69.05	99.05	14.27	33.53	72.15	87.31	108.66	142.28	8.52	19.22	40.31	49.87	66.69	102.20
Action	Purchases						Sitting						Sitting Down					
Millisecond (ms)	80	160	320	400	560	1000	80	160	320	400	560	1000	80	160	320	400	560	1000
Residual sup. [30]	30.54	52.89	86.31	99.07	121.00	169.66	22.08	38.58	64.59	75.94	96.33	145.90	27.73	47.24	79.55	93.33	117.92	170.19
DMGNN [21]	17.60	36.24	69.43	83.20	104.09	145.26	11.77	23.42	48.33	60.69	80.75	123.31	16.93	32.04	62.19	76.52	101.16	153.00
FC-GCN [29]	15.60	32.78	<u>65.72</u>	<u>79.25</u>	<u>100.19</u>	141.14	10.62	21.90	46.33	57.91	79.38	122.44	16.14	31.12	61.74	76.46	99.24	149.30
Traj-CNN [23]	14.54	31.88	66.55	80.75	103.65	141.01	10.97	21.17	45.48	57.50	78.95	120.12	16.13	<u>29.56</u>	<u>58.74</u>	<u>72.59</u>	<u>97.00</u>	146.96
STS-GCN [36]	<u>13.87</u>	<u>31.66</u>	66.00	80.04	102.46	142.46	<u>9.63</u>	<u>20.65</u>	<u>45.22</u>	<u>57.26</u>	78.96	122.03	<u>14.98</u>	29.60	59.41	73.55	98.80	149.52
MSR-GCN [6]	14.75	32.39	66.13	79.64	101.63	<u>139.16</u>	10.53	21.99	46.26	57.80	<u>78.20</u>	<u>120.04</u>	16.10	31.63	62.45	76.84	102.84	155.47
Ours	12.68	29.65	62.29	75.79	97.54	137.76	8.78	19.32	42.88	54.33	74.94	117.75	14.10	28.03	57.33	71.18	96.08	147.25
Action	Waiting						Walking Dog						Walking Together					
Millisecond (ms)	80	160	320	400	560	1000	80	160	320	400	560	1000	80	160	320	400	560	1000
Residual sup. [30]	25.78	44.52	72.29	82.44	98.79	136.76	39.19	67.36	105.56	117.96	135.99	186.09	22.03	36.08	54.91	60.30	67.89	85.19
DMGNN [21]	12.89	25.70	51.27	62.84	79.82	112.99	26.09	50.47	88.90	102.55	118.44	156.09	13.76	25.55	44.49	53.47	59.41	79.06
FC-GCN [29]	11.43	23.99	50.06	61.48	78.15	108.77	23.39	46.17	83.47	95.96	<u>110.98</u>	146.24	10.47	21.04	38.47	45.19	54.71	66.96
Traj-CNN [23]	10.51	<u>21.76</u>	<u>45.79</u>	<u>56.29</u>	<u>73.36</u>	<u>104.53</u>	21.30	43.29	80.77	94.50	115.56	153.50	10.30	21.11	38.48	44.82	54.78	68.00
STS-GCN [36]	<u>10.00</u>	21.93	46.98	58.22	76.39	107.68	20.79	43.56	81.81	95.20	114.36	151.92	<u>10.06</u>	<u>20.69</u>	39.07	46.00	54.92	<u>62.91</u>
MSR-GCN [6]	10.68	23.06	48.25	59.23	76.33	106.27	20.65	42.88	<u>80.35</u>	<u>93.31</u>	111.89	148.24	10.56	20.92	37.40	<u>43.85</u>	<u>52.94</u>	65.94
Ours	8.71	20.15	44.28	55.25	73.19	105.66	19.64	41.82	77.61	90.24	109.84	147.68	9.07	19.79	36.33	42.67	50.54	61.22
Action	Discussion						Posing						Taking Photo					
Millisecond (ms)	80	160	320	400	560	1000	80	160	320	400	560	1000	80	160	320	400	560	1000
Residual sup. [30]	27.74	48.22	79.13	90.02	106.71	134.22	32.99	59.71	104.87	123.67	158.74	300.18	21.53	37.30	63.83	75.78	95.70	145.82
DMGNN [21]	14.77	30.86	62.05	75.26	93.24	123.67	15.40	32.07	67.36	84.19	113.60	171.56	11.49	23.07	46.89	58.46	78.20	121.69
FC-GCN [29]	12.50	27.40	58.51	71.68	91.61	121.53	13.66	29.89	66.62	84.05	113.56	171.31	9.88	20.89	44.95	56.58	76.52	119.33
Traj-CNN [23]	11.74	<u>26.30</u>	57.29	70.36	91.45	122.66	12.09	<u>26.94</u>	<u>62.44</u>	<u>79.33</u>	<u>108.36</u>	170.86	10.43	20.64	44.37	55.83	76.78	120.11
STS-GCN [36]	<u>11.39</u>	26.41	57.78	71.08	91.16	120.79	<u>11.61</u>	27.60	63.85	81.23	111.68	<u>168.41</u>	<u>9.15</u>	<u>19.87</u>	<u>43.42</u>	<u>54.99</u>	<u>76.15</u>	<u>118.76</u>
MSR-GCN [6]	11.98	26.76	<u>57.08</u>	<u>69.74</u>	<u>88.59</u>	<u>117.59</u>	12.79	29.38	66.95	85.01	116.27	174.33	9.89	21.01	44.56	56.30	77.97	121.91
Ours	9.98	24.37	54.53	67.40	87.00	116.30	10.08	25.40	60.60	77.34	106.54	163.31	8.41	18.84	42.00	53.50	74.50	117.91

Table 5: Comparison Summaries of Average MPJPE and Parameter Numbers

Model	DSTD-C	DSTD-D	DSTD-R	DSTD-P	DSTD-GCN
MPJPE	39.65	43.06	47.36	35.84	35.51

4.5 RQ3: Ablation Study

In this section, we analyze some key elements in our methods in Human3.6M or CMU Mocap dataset.

Table 3: Comparisons of prediction results on CMU Mocap dataset. The best results are highlighted in bold, while the second best results are shown in underline.

Action	Basketball						Basketball Signal						Directing Traffic					
Millisecond (ms)	80	160	320	400	560	1000	80	160	320	400	560	1000	80	160	320	400	560	1000
Residual sup. [30]	29.5	53.05	91.22	106.03	128.74	157.38	14.63	22.07	39.07	46.56	59.98	89.93	21.77	38.78	70.45	85.3	110.29	165.13
DMGNN [21]	14.97	27.07	49.36	61.45	84.83	145.18	4.91	8.78	15.93	19.60	27.43	47.28	10.62	19.63	36.03	44.34	62.87	115.71
FC-GCN [29]	11.67	21.09	40.70	50.58	68.03	95.66	3.35	6.23	13.48	17.87	27.34	51.88	6.78	13.36	29.57	39.06	59.64	112.83
Traj-CNN [23]	11.84	19.12	<u>36.72</u>	46.02	62.47	95.76	4.42	6.20	12.29	16.19	25.48	51.76	6.95	<u>11.03</u>	<u>25.89</u>	40.99	54.76	112.43
STS-GCN [36]	<u>10.23</u>	<u>18.67</u>	<u>36.93</u>	<u>45.98</u>	<u>61.19</u>	<u>91.36</u>	<u>2.96</u>	<u>5.52</u>	<u>12.12</u>	<u>16.12</u>	<u>25.15</u>	<u>50.88</u>	<u>5.95</u>	<u>11.99</u>	<u>27.55</u>	<u>36.75</u>	<u>57.05</u>	<u>111.53</u>
MSR-GCN [6]	10.28	18.94	37.68	47.03	62.01	86.27	3.04	5.63	12.51	16.61	25.46	50.04	6.13	12.61	29.39	39.24	<u>50.49</u>	114.58
Ours	9.60	17.64	35.44	44.43	59.97	<u>88.44</u>	2.57	4.72	10.37	13.86	21.85	46.17	5.02	10.01	23.35	31.40	49.28	99.57

Action	Running						Soccer						Walking					
Millisecond (ms)	80	160	320	400	560	1000	80	160	320	400	560	1000	80	160	320	400	560	1000
Residual sup.[30]	23.46	39.94	62.26	67.46	73.21	78.16	26.51	46.98	81.45	96.18	117.9	139.06	14.61	22.87	36.09	40.90	51.10	69.49
DMGNN[21]	17.55	30.09	45.74	49.34	53.65	81.60	17.64	31.86	56.81	68.84	92.70	130.80	12.23	21.89	36.03	41.32	51.46	64.68
FC-GCN [29]	15.03	25.21	39.05	42.36	43.28	53.56	13.62	24.30	44.40	54.31	73.14	111.64	6.74	11.09	18.08	20.95	25.16	32.38
Traj-CNN [23]	14.39	23.41	37.51	39.51	40.68	51.38	13.46	21.25	38.65	47.26	<u>62.66</u>	<u>97.33</u>	7.69	11.28	18.02	20.62	25.67	40.35
STS-GCN [36]	13.26	21.84	33.98	37.71	40.95	<u>44.76</u>	11.30	20.45	39.04	48.88	69.12	102.54	6.87	11.29	18.13	21.06	26.12	37.86
MSR-GCN [6]	<u>13.17</u>	20.91	29.87	33.35	38.22	<u>43.57</u>	<u>10.92</u>	19.39	37.41	<u>47.01</u>	65.26	101.86	<u>6.39</u>	10.25	<u>16.89</u>	20.05	<u>25.49</u>	36.82
Ours	12.04	<u>20.97</u>	<u>33.71</u>	<u>37.35</u>	<u>39.82</u>	43.55	10.25	18.96	36.79	45.65	62.29	96.93	6.34	<u>10.35</u>	16.09	18.62	23.28	<u>33.56</u>

Action	Jumping						Wash Window					
Millisecond (ms)	80	160	320	400	560	1000	80	160	320	400	560	1000
Residual sup.[30]	30.18	53.02	89.35	103.9	125.55	160.49	19.32	31.77	56.05	66.00	83.62	125.87
DMGNN[21]	19.47	36.77	67.42	81.28	105.62	148.53	9.10	16.90	32.55	41.13	57.09	97.08
FC-GCN [29]	17.10	32.06	59.82	72.51	94.33	127.20	5.87	11.33	24.14	30.95	43.44	66.93
Traj-CNN [23]	<u>14.88</u>	<u>27.01</u>	<u>55.31</u>	71.72	94.23	126.97	6.64	11.04	24.14	31.22	44.19	71.34
STS-GCN [36]	15.66	30.63	59.13	71.87	93.32	125.94	5.44	<u>10.84</u>	23.90	<u>30.72</u>	<u>44.00</u>	71.42
MSR-GCN [6]	15.19	28.86	55.98	<u>69.12</u>	<u>92.40</u>	126.18	<u>5.41</u>	<u>10.94</u>	24.51	31.80	45.14	70.19
Ours	12.81	26.05	54.62	68.47	91.83	<u>126.07</u>	4.75	9.53	21.98	28.99	42.48	<u>68.93</u>

Table 4: Comparison Summaries of Average MPJPE and Parameter Numbers

Model	Human3.6M							Params.	CMU Mocap							Params.
	Average MPJPE								Average MPJPE							
	80	160	320	400	560	1000	80		160	320	400	560	1000			
Residual sup. [30]	25.91	44.36	71.86	82.35	99.90	144.44	3.42M	22.50	38.56	65.74	76.54	93.80	123.19	3.46M		
DMGNN [21]	14.67	28.91	55.51	67.44	84.04	129.06	46.93M	13.31	24.12	42.48	50.91	66.96	103.86	46.94M		
FC-GCN [29]	12.68	26.06	52.29	63.58	81.17	114.14	2.55M	10.02	18.08	33.66	41.07	54.29	81.51	2.70M		
Traj-CNN [23]	12.09	24.86	50.74	61.95	80.78	114.92	2.42M	10.03	16.29	31.07	39.19	51.14	78.69	2.42M		
STS-GCN [36]	<u>11.43</u>	<u>24.77</u>	<u>51.16</u>	<u>62.58</u>	<u>81.12</u>	<u>113.78</u>	<u>0.39M</u>	8.95	16.40	31.35	38.64	52.11	80.27	<u>0.46M</u>		
MSR-GCN [6]	12.11	25.56	51.64	62.93	81.14	114.19	6.30M	<u>8.81</u>	<u>15.91</u>	<u>30.45</u>	<u>37.99</u>	<u>50.54</u>	<u>76.69</u>	6.37M		
Ours	10.38	23.34	48.77	59.84	77.81	111.02	0.18M	7.92	14.78	29.04	36.09	48.85	76.39	0.20M		

4.5.1 Effect of Constrained Dynamic Correlation Modeling Strategy.

We investigate our proposed constrained dynamic modeling strategy. We design three ablation variants of DSTD-GCN: (1) DSTD-C: DSTD-GCN only with constrained correlation updating in DG-GC and DT-GC; (2) DSTD-D: DSTD-GCN only with dynamic correlation adjustment in DG-GC and DT-GC. (3) DSTD-R: constrained correlation is used to update dynamic correlations in the feature adjustment phase. The detail results are shown in Table 5. First, we study the relationships between the constrained correlation and the dynamic correlation. Comparing the prediction error of DSTD-C and DSTD-D: we observe that DSTD-C outperforms DSTD-D with

lower prediction error, indicating that constrained correlations are more important for accurate motion prediction. Then, we study the updating strategy by comparing DSTD-R and DSTD-GCN. We find that the dynamic correlation complete the constrained correlations but not vice versa.

4.5.2 Effect of Prior Connections. We analyze the effects of prior connections in constrained correlations. We remove all predefined correlations in DSTD-GCN and obtain DSTD-P. The reduction of prior connections (0.33) is much less than reduction of constrained dynamic correlation modeling (4.14). The prediction performance

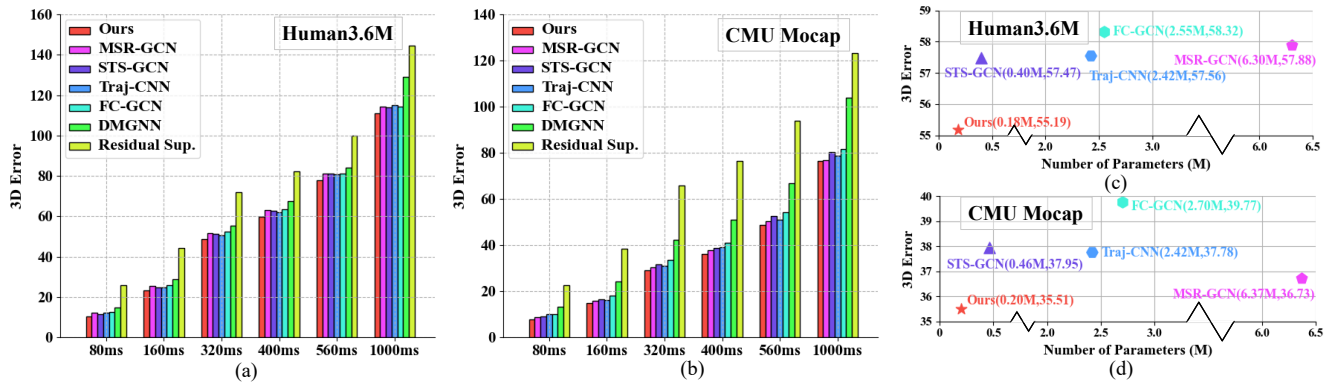


Figure 6: Comparisons Summaries on the Human3.6M and the CMU-Mocap dataset. (a) and (b) show average prediction error at different forecast times. (c) and (d) show average prediction error and model parameters.

is slightly dropped compared with DSTD-GCN. Note that other baselines don't get prior connections, DSTD-P still outperforms state-of-the-art baseline MSR-GCN by 0.79, indicating the effectiveness of our proposed spatiotemporal correlation modeling.

5 CONCLUSIONS

In this work, we propose a novel Dynamic SpatioTemporal Decompose Graph Convolutions (DSTD-GC) for human motion prediction. DSTD-GC deploys constrained dynamic correlation modeling strategy, which extends conventional graph convolutions by combining constrained correlations from training or prior knowledge and dynamic correlations from input motion sequences. We make mathematical analysis and conduct extensive experiment to illustrate the power spatiotemporal modeling capability of DSTD-GC, which break certain constraints of state-of-the-art spatiotemporal graph convolutions. With this strategy, we propose DSTD-GCN which outperforms other state-of-the-art methods in prediction accuracy with fewest parameters.

REFERENCES

- [1] Emre Aksan, Manuel Kaufmann, Peng Cao, and Otmar Hilliges. 2021. A spatio-temporal transformer for 3D human motion prediction. In *2021 International Conference on 3D Vision (3DV)*. IEEE, 565–574.
- [2] Amal Fahad Al-aqel and Murtaza Ali Khan. 2020. Attention mechanism for human motion prediction. In *2020 3rd International Conference on Computer Applications & Information Security (ICCAIS)*. IEEE, 1–6.
- [3] Yujun Cai, Lin Huang, Yiwei Wang, Tat-Jen Cham, Jianfei Cai, Junsong Yuan, Jun Liu, Xu Yang, Yiheng Zhu, Xiaohui Shen, et al. 2020. Learning progressive joint propagation for human motion prediction. In *European Conference on Computer Vision*. Springer, 226–242.
- [4] Qiongjie Cui, Huaijiang Sun, Yue Kong, Xiaoqian Zhang, and Yanmeng Li. 2021. Efficient human motion prediction using temporal convolutional generative adversarial network. *Information Sciences* 545 (2021), 427–447.
- [5] Qiongjie Cui, Huaijiang Sun, and Fei Yang. 2020. Learning dynamic relationships for 3d human motion prediction. In *Proceedings of the IEEE/CVF conference on computer vision and pattern recognition*. 6519–6527.
- [6] Lingwei Dang, Yongwei Nie, Chengjiang Long, Qing Zhang, and Guiqing Li. 2021. MSR-GCN: Multi-Scale Residual Graph Convolution Networks for Human Motion Prediction. In *Proceedings of the IEEE/CVF International Conference on Computer Vision*. 11467–11476.
- [7] Tyler Derr, Yao Ma, and Jiliang Tang. 2018. Signed graph convolutional networks. In *2018 IEEE International Conference on Data Mining (ICDM)*. IEEE, 929–934.
- [8] Katerina Fragkiadaki, Sergey Levine, Panna Felsen, and Jitendra Malik. 2015. Recurrent network models for human dynamics. In *Proceedings of the IEEE international conference on computer vision*. 4346–4354.
- [9] Liang-Yan Gui, Yu-Xiong Wang, Xiaodan Liang, and José MF Moura. 2018. Adversarial geometry-aware human motion prediction. In *Proceedings of the European Conference on Computer Vision (ECCV)*. 786–803.
- [10] Xiao Guo and Jongmoo Choi. 2019. Human motion prediction via learning local structure representations and temporal dependencies. In *Proceedings of the AAAI Conference on Artificial Intelligence*, Vol. 33. 2580–2587.
- [11] Kaiming He, Xiangyu Zhang, Shaoqing Ren, and Jian Sun. 2015. Delving deep into rectifiers: Surpassing human-level performance on imagenet classification. In *Proceedings of the IEEE international conference on computer vision*. 1026–1034.
- [12] Alejandro Hernandez, Jurgen Gall, and Francesc Moreno-Noguer. 2019. Human motion prediction via spatio-temporal inpainting. In *Proceedings of the IEEE/CVF International Conference on Computer Vision*. 7134–7143.
- [13] Catalin Ionescu, Dragoș Papava, Vlad Olaru, and Cristian Sminchisescu. 2013. Human3.6m: Large scale datasets and predictive methods for 3d human sensing in natural environments. *IEEE transactions on pattern analysis and machine intelligence* 36, 7 (2013), 1325–1339.
- [14] Qihong Ke, Mohammed Bannamou, Hossein Rahmani, Senjian An, Ferdous Sohel, and Farid Boussaid. 2019. Learning latent global network for skeleton-based action prediction. *IEEE Transactions on Image Processing* 29 (2019), 959–970.
- [15] Diederik P Kingma and Jimmy Ba. 2014. Adam: A method for stochastic optimization. *arXiv preprint arXiv:1412.6980* (2014).
- [16] Thomas N Kipf and Max Welling. 2016. Semi-supervised classification with graph convolutional networks. *arXiv preprint arXiv:1609.02907* (2016).
- [17] Yu Kong and Yun Fu. 2018. Human action recognition and prediction: A survey. *arXiv preprint arXiv:1806.11230* (2018).
- [18] Jogendra Nath Kundu, Maharshi Gor, and R Venkatesh Babu. 2019. Bihmpgan: Bidirectional 3d human motion prediction gan. In *Proceedings of the AAAI conference on artificial intelligence*, Vol. 33. 8553–8560.
- [19] Andreas M Lehrmann, Peter V Gehler, and Sebastian Nowozin. 2014. Efficient nonlinear markov models for human motion. In *Proceedings of the IEEE Conference on Computer Vision and Pattern Recognition*. 1314–1321.
- [20] Chen Li, Zhen Zhang, Wee Sun Lee, and Gim Hee Lee. 2018. Convolutional sequence to sequence model for human dynamics. In *Proceedings of the IEEE Conference on Computer Vision and Pattern Recognition*. 5226–5234.
- [21] Maosen Li, Siheng Chen, Yangheng Zhao, Ya Zhang, Yanfeng Wang, and Qi Tian. 2020. Dynamic multiscale graph neural networks for 3d skeleton based human motion prediction. In *Proceedings of the IEEE/CVF Conference on Computer Vision and Pattern Recognition*. 214–223.
- [22] Maosen Li, Siheng Chen, Yangheng Zhao, Ya Zhang, Yanfeng Wang, and Qi Tian. 2021. Multiscale Spatio-Temporal Graph Neural Networks for 3D Skeleton-Based Motion Prediction. *IEEE Transactions on Image Processing* 30 (2021), 7760–7775.
- [23] Xiaoli Liu, Jianqin Yin, Jin Liu, Pengxiang Ding, Jun Liu, and Huaping Liu. 2020. Trajectorycnn: a new spatio-temporal feature learning network for human motion prediction. *IEEE Transactions on Circuits and Systems for Video Technology* 31, 6 (2020), 2133–2146.
- [24] Zhenguang Liu, Kedi Lyu, Shuang Wu, Haipeng Chen, Yanbin Hao, and Shouling Ji. 2021. Aggregated multi-gans for controlled 3d human motion prediction. In *Proceedings of the AAAI Conference on Artificial Intelligence*, Vol. 35. 2225–2232.
- [25] Zhenguang Liu, Pengxiang Su, Shuang Wu, Xuanjing Shen, Haipeng Chen, Yanbin Hao, and Meng Wang. 2021. Motion prediction using trajectory cues. In *Proceedings of the IEEE/CVF International Conference on Computer Vision*. 13299–13308.

- [26] Zhenguang Liu, Shuang Wu, Shuyuan Jin, Qi Liu, Shijian Lu, Roger Zimmermann, and Li Cheng. 2019. Towards natural and accurate future motion prediction of humans and animals. In *Proceedings of the IEEE/CVF Conference on Computer Vision and Pattern Recognition*. 10004–10012.
- [27] Kedi Lyu, Zhenguang Liu, Shuang Wu, Haipeng Chen, Xuhong Zhang, and Yuyu Yin. 2021. Learning Human Motion Prediction via Stochastic Differential Equations. In *Proceedings of the 29th ACM International Conference on Multimedia*. 4976–4984.
- [28] Wei Mao, Miaomiao Liu, and Mathieu Salzmann. 2020. History repeats itself: Human motion prediction via motion attention. In *European Conference on Computer Vision*. Springer, 474–489.
- [29] Wei Mao, Miaomiao Liu, Mathieu Salzmann, and Hongdong Li. 2019. Learning trajectory dependencies for human motion prediction. In *Proceedings of the IEEE/CVF International Conference on Computer Vision*. 9489–9497.
- [30] Julieta Martinez, Michael J Black, and Javier Romero. 2017. On human motion prediction using recurrent neural networks. In *Proceedings of the IEEE conference on computer vision and pattern recognition*. 2891–2900.
- [31] Brian Paden, Michal Čáp, Sze Zheng Yong, Dmitry Yershov, and Emilio Frazzoli. 2016. A survey of motion planning and control techniques for self-driving urban vehicles. *IEEE Transactions on intelligent vehicles* 1, 1 (2016), 33–55.
- [32] Adam Paszke, Sam Gross, Francisco Massa, Adam Lerer, James Bradbury, Gregory Chanan, Trevor Killeen, Zeming Lin, Natalia Gimelshein, Luca Antiga, et al. 2019. Pytorch: An imperative style, high-performance deep learning library. *Advances in neural information processing systems* 32 (2019).
- [33] Dario Pavlo, Christoph Feichtenhofer, Michael Auli, and David Grangier. 2020. Modeling human motion with quaternion-based neural networks. *International Journal of Computer Vision* 128, 4 (2020), 855–872.
- [34] Guocheng Qian, Abdulullah Abualshour, Guohao Li, Ali Thabet, and Bernard Ghanem. 2021. Pu-gcn: Point cloud upsampling using graph convolutional networks. In *Proceedings of the IEEE/CVF Conference on Computer Vision and Pattern Recognition*. 11683–11692.
- [35] Xiangbo Shu, Liyan Zhang, Guo-Jun Qi, Wei Liu, and Jinhui Tang. 2021. Spatiotemporal co-attention recurrent neural networks for human-skeleton motion prediction. *IEEE Transactions on Pattern Analysis and Machine Intelligence* (2021).
- [36] Theodoros Sofianos, Alessio Sampieri, Luca Franco, and Fabio Galasso. 2021. Space-Time-Separable Graph Convolutional Network for Pose Forecasting. In *Proceedings of the IEEE/CVF International Conference on Computer Vision*. 11209–11218.
- [37] Pengxiang Su, Zhenguang Liu, Shuang Wu, Lei Zhu, Yifang Yin, and Xuanjing Shen. 2021. Motion Prediction via Joint Dependency Modeling in Phase Space. In *Proceedings of the 29th ACM International Conference on Multimedia*. 713–721.
- [38] Yongyi Tang, Lin Ma, Wei Liu, and Weishi Zheng. 2018. Long-term human motion prediction by modeling motion context and enhancing motion dynamic. *arXiv preprint arXiv:1805.02513* (2018).
- [39] Graham W Taylor, Leonid Sigal, David J Fleet, and Geoffrey E Hinton. 2010. Dynamical binary latent variable models for 3d human pose tracking. In *2010 IEEE Computer Society Conference on Computer Vision and Pattern Recognition*. IEEE, 631–638.
- [40] Nikolaus F Troje. 2002. Decomposing biological motion: A framework for analysis and synthesis of human gait patterns. *Journal of vision* 2, 5 (2002), 2–2.
- [41] Vaibhav V Unhelkar, Przemyslaw A Lasota, Quirin Tyroller, Rares-Darius Buhai, Laurie Marceau, Barbara Deml, and Julie A Shah. 2018. Human-aware robotic assistant for collaborative assembly: Integrating human motion prediction with planning in time. *IEEE Robotics and Automation Letters* 3, 3 (2018), 2394–2401.
- [42] Hongsong Wang, Jian Dong, Bin Cheng, and Jiashi Feng. 2021. PVRED: A Position-Velocity Recurrent Encoder-Decoder for Human Motion Prediction. *IEEE Transactions on Image Processing* 30 (2021), 6096–6106.
- [43] Sijie Yan, Yuanjun Xiong, and Dahua Lin. 2018. Spatial temporal graph convolutional networks for skeleton-based action recognition. In *Thirty-second AAAI conference on artificial intelligence*.
- [44] Bing Yu, Haoteng Yin, and Zhanxing Zhu. 2017. Spatio-temporal graph convolutional networks: A deep learning framework for traffic forecasting. *arXiv preprint arXiv:1709.04875* (2017).